Determination of effective brain connectivity from activity correlations

J. N. MacLaurin and P. A. Robinson
School of Physics, University of Sydney, New South Wales 2006, Australia,
and Center for Integrative Brain Function, University of Sydney, New South Wales 2006, Australia

(Received 12 May 2017; revised manuscript received 12 February 2019; published 15 April 2019)

Effective connectivity embodied in transfer functions is derived from symmetric-network activity correlations under task-free conditions via a recent causal spectral factorization method. This generalizes previous covariance-based analyses to include frequency dependencies and time delays. Results are verified against analytic solutions of equations that have reproduced many aspects of experimental brain dynamics and against cases of more complex connectivity. Robustness to noise is also demonstrated.

DOI: 10.1103/PhysRevE.99.042404

Complex networks occur in many fields, including neuroscience, communications, the Internet, genetics, ecology, and economics [1–6]. Many networks, such as those in economics and the brain, have connectivities that are hard to observe directly or can only be studied in their normal state via the activity they support. This is especially true of *effective* connectivities that measure strengths of active connections, rather than all underlying structural connections [3,4]. In the brain, relationships between network structure and dynamics are essential to understanding signal propagation [2–4,7–16] and are central to large-scale initiatives such as the Human Connectome Project, the U.S. BRAIN Initiative, and the European Human Brain Project.

Recent work showed that symmetric effective mesoscale and macroscale (0.5 mm and above) brain connectivity can be determined from the covariance matrix of the activity they support [15,17,18], a result that generalizes to other networks. This result relies on matrix diagonalization methods and neural field theory (NFT) results that showed how to compute activity from effective connectivity and how to relate NFT propagators to direct effective connection matrices (deCMs) [17,18], which measure connection strengths between brain regions, and to total eCMs (teCMs), which include indirect influences and are equivalent to transfer functions; NFT functional CMs (fCMs) are then calculated as two-point activity correlations [17,18]. Each row and column of a CM represents a brain region, while the entries represent connection strengths between them [2–4].

Using general linear NFT [17,19] for signals that are not strong enough to be nonlinear, without specializing to a particular form, we recently showed that the deCM and teCM correspond to bare and dressed propagators, respectively, and can be used to compute the fCM [17,20]. Later, we showed that symmetric deCMs can be determined from the covariance matrix under task-free conditions, which is the most common situation [18]. This enabled corresponding strengths of connections to be determined, including those of connections that could not be measured reliably by methods such as magnetic resonance imaging (MRI) diffusion imaging.

Key aspects missing from most attempts to infer eCMs from fCMs are treatment of time delays and frequency dependence. These are straightforward to include in the forward problem, but covariances are symmetric and do not contain temporal information. Hence, these most common fCMs cannot be used to infer delays or frequency dependencies, which are critical to many brain phenomena. Correlation matrices potentially carry the missing information and have been used as generalized fCMs [17,21]. A recent paper [21] introduced a method for approximately inferring the form of deCMs by adjusting some of their entries to get the best possible fit of their predicted fCMs to data. However, this was restricted to one dynamical model and the authors noted difficulties in choosing which entries to adjust, especially because a 1000-node network has $\sim 10^6$ CM entries. Methods for inferring links in discrete networks without self-connections [22] and biomolecular networks [23] have also been explored recently, as have complementary methods for some classes of nonlinear networks [24–27].

In this article we show how to invert the correlation matrix of linear activity in a symmetric brain network to determine its teCM, including frequency dependencies and time delays. We first identify the teCM with the dressed propagator or transfer function [17]. The Fourier transform of the correlation function is then expressed in terms of the transfer function, which is found via Cholesky factorization of the correlation matrix at each frequency, then causality is imposed via a recent iterative method, and the propagator (Green function) is identified by adjusting the phases of the contributing modes to maximize the initial response to a δ function input [28–30].

We first discretize the brain into M regions to write the synaptic activity that dominates brain metabolism and measures like functional MRI and electroencephalography (EEG) [31–33] as an M-element column vector $\mathbf{\Phi}(t)$ [17,18]. In brain connectivity studies to date, M usually lies between 30 and 1000 [4]. Weak signals suffice to establish the existence of a connection between two points, and it has been extensively verified that most normal large-scale brain activity is stable and approximately linear relative to a fixed point in any case and that spontaneous activity can be closely approximated as being white-noise driven [17–20,34,35]; certainly axonal transmission between points also yields output spike

rates that are equal to input rates. Linear NFT implies

$$\mathbf{\Phi}(t) = \int_{-\infty}^{\infty} \mathbf{T}(t-t')\mathbf{N}(t')dt', \tag{1}$$

where $\mathbf{N}$ is a vector of external inputs and the propagator $\mathbf{T}$ is identified as a spatiotemporal teCM [17] and has $\mathbf{T}(\tau) = 0$ for $\tau < 0$, from the causal requirement that no influences can propagate into the past; temporally, $\mathbf{T}$ depends only on $\tau = t - t'$ if the network structure is static, which is a good approximation if it only changes on timescales much longer than those of the activity that determines the fCM. Fourier transforming Eq. (1) vs t gives

$$\mathbf{\Phi}(\omega) = \mathbf{T}(\omega)\mathbf{N}(\omega), \tag{2}$$

where ω is the angular frequency and $\mathbf{T} \to \mathbf{0}$ as $|\omega| \to \infty$ because of the limited bandwidth of physical systems. Once $\mathbf{T}$ is known, the linear response to any stimulus can be determined.

We define the fCM to be the correlation matrix of the activity at times separated by an interval [17], with

$$\mathbf{C}(\tau) = \langle \mathbf{\Phi}(t+\tau)\mathbf{\Phi}^T(t)\rangle, \tag{3}$$

where the angle brackets indicate an average over t and the superscript T denotes the transpose. We Fourier transform the quantities in Eq. (3), and use Eq. (2), to find [17]

$$\mathbf{C}(\omega) = \mathbf{T}(\omega)\mathbf{T}^\dagger(\omega), \tag{4}$$

where the dagger denotes a Hermitian conjugate and we have assumed uncorrelated white-noise inputs with

$$\langle \mathbf{N}(\omega)\mathbf{N}^\dagger(\omega)\rangle = \mathbf{I}. \tag{5}$$

The approximation (5) has yielded successful comparisons of NFT with a wide array of experimental results on the brain in "resting" states in which no dominant external stimuli are present [19]. Notably, Eq. (4) holds for the transfer function of any linear system, while Eq. (5) and the following analysis can be generalized to cases in which its right side is frequency dependent.

Because $\mathbf{C}(\tau)$ and $\mathbf{T}(\tau)$ are real, $\mathbf{C}(-\omega) = \mathbf{C}^*(\omega)$ and $\mathbf{T}(-\omega) = \mathbf{T}^*(\omega)$. Now $\mathbf{C}(\omega)$ is Hermitian, so $\mathbf{C}^\dagger(\omega) = \mathbf{C}(\omega)$ and its eigenvalues are real. These eigenvalues are also positive because the Wiener-Khintchine theorem states that $\mathbf{C}$ is the Fourier transform of the power spectrum, a positive-definite quantity. Infinitely many causal $\mathbf{T}$ can satisfy Eq. (4). To isolate the Green-function solution, we require that $\det[\mathbf{T}(t=0)]$ be maximal so that $\mathbf{T}$ represents the response to a δ-function input, which is the most temporally concentrated possible.

Here we adapt the key results of Ref. [28] to our present application; for full proofs see Ref. [28], which assumed that the correlation function is well behaved over the frequency range of interest, being continuous and square integrable, properties that are generally satisfied for physical systems. For computation, frequencies are discretized into $2F+1$ points and frequencies are rescaled to lie in the range $-\pi$ to π, with the endpoints of this range identified and $\omega_p = p\Delta\omega$ and $\Delta\omega = \pi/F$ for $p = -F, \ldots, F$; corresponding discrete times can be chosen to be $t_p = p\Delta t$ with a time step Δt. In applications Δt is the smallest resolvable scale and $F\Delta t$ must be large enough that $\mathbf{T}(t)$ is negligible at the ends of the overall time interval. The method converges as $F \to \infty$ [28].

The first step is to Cholesky factorize Eq. (4) to write

$$\mathbf{C}(\omega_p) = \mathbf{K}(\omega_p)\mathbf{K}^\dagger(\omega_p), \tag{6}$$

where $\mathbf{K}$ is a lower triangular matrix with nonnegative real diagonal elements $K_{jj}(\omega_p)$. Right multiplication of $\mathbf{K}$ by any unitary matrix $\mathbf{W}$ yields another matrix that satisfies Eq. (6), but if $\mathbf{K}$ or $\mathbf{KW}$ is inverse Fourier transformed, the corresponding propagator is not necessarily causal. Hence, the next step is to find a diagonal unitary matrix $\mathbf{W}(\omega_p)$ that transforms $\mathbf{K}$ into a matrix $\mathbf{T}^{(0)}$ whose diagonal entries are causal, with

$$\mathbf{T}^{(0)}(\omega_p) = \mathbf{K}(\omega_p)\mathbf{W}(\omega_p). \tag{7}$$

A suitable form of $\mathbf{W}$ is [28]

$$\mathbf{W}(\omega_p) = \mathrm{diag}[K^+_{jj}(\omega_p)/K_{jj}(\omega_p)], \tag{8}$$

$$K^+_{jj}(\omega_p) = \exp\left(\int_{-\pi}^{\pi} \frac{e^{i\theta}+e^{i\omega_p}}{e^{i\theta}-e^{i\omega_p}} \frac{\ln|K_{jj}(\theta)|}{4\pi} d\theta\right). \tag{9}$$

Here $K^+_{jj}(\omega_p)$ is a spectral factor of $K_{jj}(\omega_p)$, meaning that $K^+_{jj}(\omega_p)$ is causal and satisfies $|K^+_{jj}(\omega_p)| = |K_{jj}(\omega_p)|$. We use a fast Fourier transform to evaluate the right side of Eq. (9).

We must now find a unitary matrix that transforms $\mathbf{T}^{(0)}$ with causal diagonal entries into a fully causal matrix $\mathbf{T}$. The problem of finding a causal solution of Eq. (4) was first addressed over 60 years ago [36], but a recent highly efficient method is used here [28]. This finds a succession of unitary matrices $\mathbf{V}^{(j)}$, $j = 1, \ldots, M$, such that the leading $m \times m$ submatrix of

$$\mathbf{T}^{(m)}(\omega_p) = \mathbf{T}^{(0)}(\omega_p)\mathbf{V}^{(1)}(\omega_p)\cdots\mathbf{V}^{(m)}(\omega_p), \tag{10}$$

is causal. The desired propagator is $\mathbf{T}(\omega_p) = \mathbf{T}^{(M)}(\omega_p)$.

The explicit form of the unitary $\mathbf{V}^{(m)}$ is [28]

$$\mathbf{V}^{(m)}(\omega_p) = \begin{pmatrix} \mathbf{X^{(m)}}(\omega_\mathbf{p})\mathbf{X^{(m)}}(\omega_\mathbf{0})^{-1} & \mathbf{0} \\ \mathbf{0} & \mathbf{I} \end{pmatrix}, \tag{11}$$

where $\mathbf{I}$ is an $(M-m)\times(M-m)$ identity matrix. We define the elements of $\mathbf{X}^{(m)}$ such that $X^{(m)}_{jk}(t_p) = 0$ if $j \leqslant m-1$ and $p < 0$, and that $X^{(m)}_{mk}(t_p) = 0$ if $p > 0$. At the mth step we define these elements to be components of the vectors

$$\mathbf{x}_{jk} = \left[X^{(m)}_{jk}(t_0), X^{(m)}_{jk}(t_1), \ldots, X^{(m)}_{jk}(t_F)\right]^T, \tag{12}$$

$$\mathbf{x}_{mk} = \left[X^{(m)}_{mk}(t_0), X^{(m)}_{mk}(t_{-1}), \ldots, X^{(m)}_{mk}(t_{1-F}), w\right]^T, \tag{13}$$

where w is a dummy variable that only serves as a placeholder, and for $j = 1, \ldots, m-1$, with [28]

$$\mathbf{x}_{mk} = \mathbf{\Theta}^{-1}\mathbf{D}^{-1}\mathbf{\Gamma}_k(\mathbf{D}^*)^{-1}\mathbf{1}, \tag{14}$$

$$\mathbf{x}_{jk} = (\mathbf{D}^*)^{-1}\mathbf{\Gamma}^*_j\mathbf{x}_{mk} - \delta_{jk}(\mathbf{D}^*)^{-1}\mathbf{1}, \tag{15}$$

for $j = 1, \ldots, (m-1)$, $k = 1, \ldots, m$, and $\mathbf{1} = (1, 0, \ldots, 0)^T$. Here,

$$\mathbf{\Theta} = \mathbf{I} + \sum_{j=1}^{m-1} \mathbf{D}^{-1}\mathbf{\Gamma}_j(\mathbf{D}^*)^{-1}\mathbf{\Gamma}^*_j, \tag{16}$$

where $\mathbf{D}$ is an upper-triangular $(F+1)\times(F+1)$ square matrix, with elements $D_{lk}=0$ if $l>k$, and $D_{lk}=T^{(m-1)}_{mm}(t_{k-l})$ otherwise. For $j=1,\ldots,(m-1)$, $\mathbf{\Gamma}_j$ is the $(F+1)\times(F+1)$ matrix with elements $(\Gamma_j)_{kl}=0$ if $k+l>F+2$, and $(\Gamma_j)_{kl}=T^{(m-1)}_{mj}(t_{2-k-l})$ otherwise, and $\mathbf{\Gamma}_m=\mathbf{D}^*$.

The above algorithm guarantees that $\mathbf{T}^{(M)}(t_q)$ is real. This follows by first noting that $\mathbf{C}(-\omega)=\mathbf{C}(\omega)^*$, so $\mathbf{T}^{(0)}(-\omega_q)=\mathbf{T}^{(0)}(\omega_q)^*$. We then proceed inductively by supposing that $\mathbf{T}^{(m)}(t_q)$ is real for some m. This means that $\mathbf{D}$ and $\mathbf{\Gamma}_j$ are real, which means that $\mathbf{X}^{(m)}(-\omega_q)=\mathbf{X}^{(m)}(\omega_q)^*$, so $\mathbf{X}^{(m)}(t_q)$ and $\mathbf{T}^{(m+1)}(t_q)$ are thus real.

We noted above that right multiplication of $\mathbf{T}^{(M)}$ by a constant orthogonal matrix yields another solution of Eq. (4). We now restrict attention to symmetric systems and choose this multiplier to make $\mathbf{T}(\omega_0)$ symmetric, using the singular value decomposition of $\mathbf{T}^{(M)}(\omega_0)$. Writing $\mathbf{T}^{(M)}(\omega_0)=\mathbf{PD}'\mathbf{R}^T$, with $\mathbf{D}'$ diagonal, we then define

$$\mathbf{T}(\omega_p)=\mathbf{T}^{(M)}(\omega_p)\mathbf{R}\mathbf{P}^T. \tag{17}$$

The above steps yield an expression for a causal propagator, $\mathbf{T}(\omega)=\mathbf{T}^{(M)}(\omega)$, that aligns the phases of the modes of $\mathbf{T}$ to maximize $\det\mathbf{T}(t=0)$ and thus yield the system Green function (for the details of the proof see Ref. [28]). In some applications, the Fourier form suffices to explore frequency-dependent brain connectivity; otherwise, an inverse Fourier transform yields $\mathbf{T}(\tau)$. In the brain context this determines the teCM from the fCM. If one is not interested in time delays, the zero-frequency components of these matrices are proportional to the time-averaged connectivities.

At large spatial and temporal system sizes, M and F are large. The dominant computational cost derives from the calculation of the matrix $\mathbf{x}_{jk}$ in Eq. (15) m^2 times at step m. Because there are M steps and the calculation cost of the matrix multiplication in Eq. (15) is only $O(F^2)$ because $\mathbf{D}$ and $\mathbf{\Gamma}_k$ are Toeplitz, the total cost is $O(M^3F^2)$.

To demonstrate the accuracy and stability of our method on brain networks, we test it on two cases with known analytic solutions and one with more complicated connectivity. We treat one-dimensional (1D) and 2D systems of unit linear size with periodic boundary conditions and discretize them spatially and temporally as above. In each case we use known analytic and/or numerical test-case dynamics to generate a test propagator $\mathbf{T}(t)$ and calculate the resulting correlation function $\mathbf{C}(\omega)$.

In our test cases we discretize the system as described above and consider the propagator from a point in the system at $t=0$. We define the elements of $\mathbf{T}$ to be $T_{jk}(t_p)=u(x_j,x_k,t_p)$, where the vector $\mathbf{u}$ satisfies

$$\frac{1}{\gamma^2}\frac{\partial^2\mathbf{u}(t)}{\partial t^2}+\frac{2}{\gamma}\frac{\partial\mathbf{u}(t)}{\partial t}+\mathbf{u}(t) -\rho^2\nabla^2\mathbf{u}(t)-\mathbf{A}\mathbf{u}(t)=\delta(t)\mathbf{1}_k, \tag{18}$$

where $\mathbf{A}$ is a symmetric constant matrix, ∇^2 is a matrix operator that implements the spatial second derivative on the discrete grid, $\delta(t)$ is a δ function at $t=0$, and $\mathbf{1}_k$ represents a spatial δ function at a chosen stimulus point x_k. In the calculations here we use $2F=2048$. Equation (18) with $\mathbf{A}=\mathbf{0}$ and more general drive on the right has been successfully used in modeling a wide variety of brain dynamics and encompasses long-range intracortical connections with approximately exponential fall-off, as is most easily seen when it is written in integral form [19,37–39].

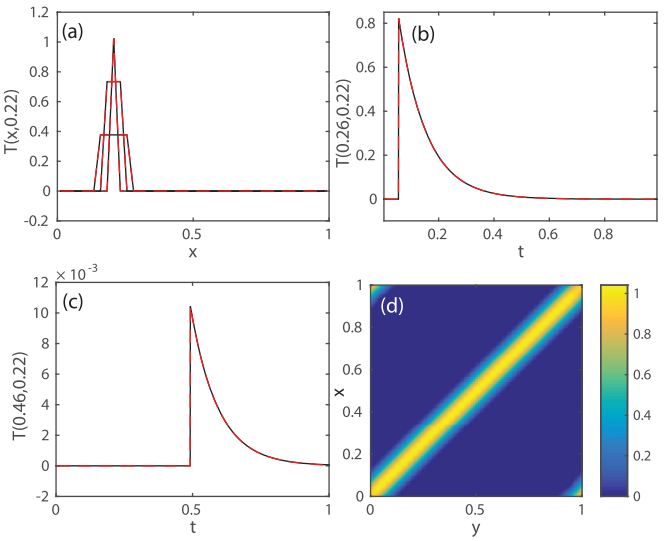

FIG. 1. One-dimensional test inversion using Eq. (18) with $\mathbf{A}=\mathbf{0}$ to generate the input $\mathbf{T}$, shown in black, for the parameters in the text; the inverted $\mathbf{T}$ is shown in red (the curves overlap at this scale). (a) The element of $\mathbf{T}$ for propagation from $x=0.22$ at $t=0$ to x and $t=0.05$, 0.1, and 0.2 (narrowest to broadest curves). (b) The element of $\mathbf{T}$ for propagation from $x=0.22$ at $t=0$ to $x=0.26$ vs t. (c) The element of $\mathbf{T}$ for propagation from $x=0.22$ at $t=0$ to $x=0.46$ vs t. (d) T for propagation from x at $t=0$ to y at $t=0.15$.

In the first test case we set $M=41$, $\gamma=10$, $\rho^2=0.05$, and $\mathbf{A}=\mathbf{0}$ in Eq. (18), which is the telegrapher's equation that is widely used to represent brain activity [19,37,40]. The 1D solution is a flat-topped response [41] that spreads at a speed of $v=\rho\gamma$ and decays like $\exp(-\gamma t)$, as seen in Figs. 1(a)–1(c). Figures 1(b) and 1(c) show there is no response at x until $t=|x-x_k|/v$, followed by exponential decay. The inversion is found to have an absolute error of $\sim10^{-3}$.

The second test case solves Eq. (18) with $\mathbf{A}=\mathbf{0}$ except for two symmetric unit entries that link the spatial points at 0.24 and 0.73 to represent instantaneous long-range reciprocal coupling, with other parameters as in the first case; more general cases follow directly by adding more such reciprocal connections. Figure 2 shows that the solutions are similar to those in Fig. 1, except that the additional connections cause activity to jump from $x=0.24$ to $x=0.73$ as the pulses pass over the former. Secondary waves of activity then emanate from $x=0.73$ and jump back to $x=0.24$, causing the off-center peaks in the response. The accuracy of the inversion is again high, but some small deviations are seen in Fig. 2(c) prior to the arrival of the main response; these are due to roundoff effects due to the sharp discontinuities in the stimulus and propagator and are of the same order as the negative discrepancy seen in Fig. 2(b).

The third test case solves the telegrapher's equation on a 25×25 grid in 2D, with $M=625$ points, $\gamma=25$, and other parameters as in Fig. 1. The analytic result in Fig. 3(a) shows the expected spreading ring of activity [37], concentrated at

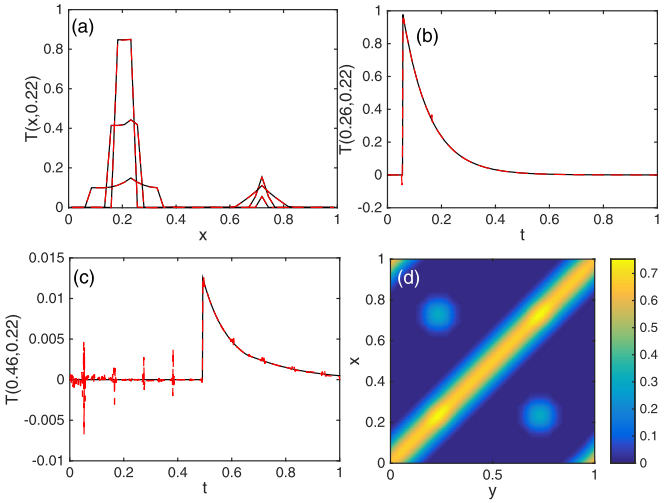

FIG. 2. One-dimensional test inversion using Eq. (18) and the parameters of Fig. 1, but with $\mathbf{A} \neq \mathbf{0}$ for unit entries corresponding to bidirectional connections between $x = 0.24$ and $x = 0.73$. The input $\mathbf{T}$ is shown in black, and the inverted $\mathbf{T}$ is shown in red. (a) The element of $\mathbf{T}$ at $t = 0.1$, 0.2, and 0.3 for propagation from $x = 0.22$ at $t = 0$ to x at $t = 0.1$, 0.2, and 0.3 (narrowest to broadest curves). (b) The element of $\mathbf{T}$ for propagation from $x = 0.22$ at $t = 0$ to $x = 0.26$ vs t. (c) The element of $\mathbf{T}$ for propagation from $x = 0.22$ at $t = 0$ to $x = 0.46$ vs t. (d) T for propagation from x at $t = 0$ to y at $t = 0.15$.

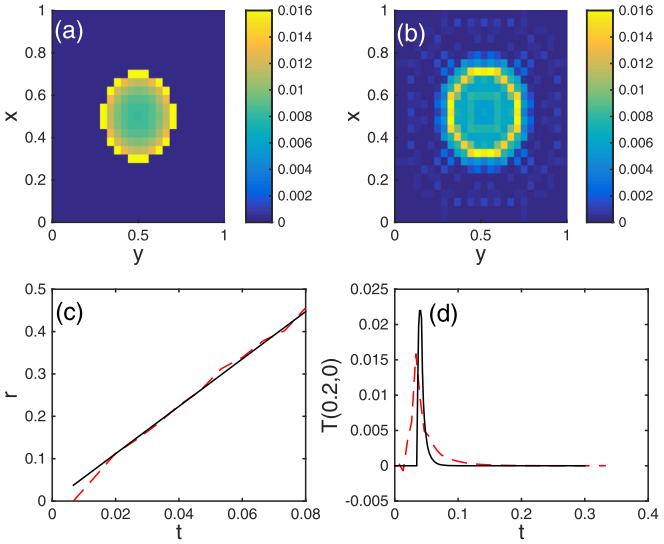

FIG. 3. Two-dimensional test inversion using Eq. (18) with $M = 625$, $\gamma = 25$, $\mathbf{A} = \mathbf{0}$, and other parameters as in Fig. 1. (a) Analytic $\mathbf{T}$ to point (x, y) at $t = 0.15$ from the origin at $t = 0$. (b) Inverted $\mathbf{T}$ to point (y, x) at $t = 0.15$ from (0,0) at $t = 0$. (c) Azimuthally averaged radial position of the peak response vs t, with analytic $\mathbf{T}$ shown as a solid black curve and inverted $\mathbf{T}$ shown as a dashed red curve. (d) Azimuthally averaged $\mathbf{T}$ vs t for propagation to a distance 0.2 from the stimulus point.

the leading edge at radius $r = vt$ with a decreasing tail behind it, of amplitude $\propto (v^2t^2 - r^2)^{-1/2} \exp(-\gamma t)$. Figure 3(b) shows that the inversion provides a good approximation to the analytic result, aside from residual fourfold symmetry from the grid, that decreases as the discretization is made finer. In particular, in Fig. 3(c) we see that the radial position of the peak response agrees closely between the inputted and inverted cases. It is seen that the inversion preserves the profile of the response, with the propagator being approximately zero before the response arrives and decreasing as expected after the peak. The peak is slightly broader and lower in amplitude in Fig. 3(d) due to discretization.

To check the robustness of the inversion to experimental noise, we also carry out calculations in which Gaussian noise is added to $\mathbf{C}$ before inversion, of a form that preserves the symmetry properties of $\mathbf{C}$. Then the algorithm is applied to see how closely the original $\mathbf{T}$ can be recovered from the noisy $\mathbf{C}$. The results (not shown) imply that the norm of the error in the inversion is linear in the norm of the perturbation added to $\mathbf{C}$, so the method is robust to low-level noise.

We have shown that the correlation-based fCM $\mathbf{C}$ can be used to infer the causal teCM or transfer matrix $\mathbf{T}$ in symmetric systems, including time delays and frequency dependencies, using a recent causal spectral factorization that we demonstrate to be accurate and robust. These results generalize prior analyses [18] and can be used to analyze brain networks obtained via EEG and magnetoencephalography measurements. Once $\mathbf{T}$ is known it can be used to predict the linear response to any stimulus, including those seen in evoked response experiments and spontaneous EEG.

The present method differs from prior techniques for related problems, including those mentioned at the start of this paper and dynamic causal modeling [21,42,43], which often require a specific dynamic model to be assumed at each node and cannot always handle networks with large numbers of nodes. In contrast, our method assumes no specific dynamics aside from approximate linearity and can treat large networks; for example, the case in Fig. 3 uses 625 nodes. This should motivate more extensive measurement and analysis of brain activity correlations. The method is also relevant to other complex networks discussed in the introduction, whose structure is difficult to measure directly, but is more readily probed via the activity they support. Qualitatively, the present method is equivalent to inferring the response of a drumhead to the impact of a single raindrop (the teCM) by measuring only the correlations of its vibrations when excited by a rainstorm (the fCM).

The Australian Research Council supported this work under Laureate Fellowship Grant No. FL1401000225 and Center of Excellence Grant No. CE140100007.

[1] S. Boccaletti, V. Latora, Y. Moreno, M. Chavez, and D.-U. Hwang, Phys. Rep. **424**, 175 (2006).
[2] K. J. Friston, Brain Connectivity **1**, 13 (2011).
[3] E. Bullmore and O. Sporns, Nat. Rev. Neurosci. **10**, 186 (2009).

[4] O. Sporns, *Networks of the Brain* (MIT, Cambridge, MA, 2011).
[5] R. Albert and A. L. Barabasi, Rev. Mod. Phys. **74**, 47 (2002).
[6] M. Barthélemy, Phys. Rep. **499**, 1 (2011).
[7] O. Sporns, G. Tononi, and G. M. Edelman, Cereb. Cortex **10**, 127 (2000).
[8] C. J. Honey, R. Kötter, M. Breakspear, and O. Sporns, Proc. Natl. Acad. Sci. USA **104**, 10240 (2007).
[9] P. A. Robinson, J. A. Henderson, E. Matar, P. Riley, and R. T. Gray, Phys. Rev. Lett. **103**, 108104 (2009).
[10] J. A. Henderson and P. A. Robinson, Phys. Rev. Lett. **107**, 018102 (2011).
[11] M. Rubinov, O. Sporns, J.-P. Thivierge, and M. Breakspear, PLoS Comput. Biol. **7**, e1002038 (2011).
[12] M. G. Kitzbichler, M. L. Smith, S. R. Christensen, and E. Bullmore, PLoS Comput. Biol. **5**, e1000314 (2009).
[13] S. A. Knock, A. R. McIntosh, O. Sporns, R. Kötter, P. Hagmann, and V. K. Jirsa, J. Neurosci. Methods **183**, 86 (2009).
[14] M. D. Grecius, K. Supekar, V. Menon, and R. F. Dougherty, Cereb. Cortex **19**, 72 (2009).
[15] R. F. Galán, PLoS ONE **3**, e2148 (2008).
[16] C. J. Honey, J.-P. Thivierge, and O. Sporns, NeuroImage **52**, 766 (2010).
[17] P. A. Robinson, Phys. Rev. E **85**, 011912 (2012).
[18] P. A. Robinson, S. Sarkar, G. M. Pandejee, and J. A. Henderson, Phys. Rev. E **90**, 012707 (2014).
[19] G. Deco, V. K. Jirsa, P. A. Robinson, M. Breakspear, and K. Friston, PLoS Comput. Biol. **4**, e1000092 (2008).
[20] P. A. Robinson, Phys. Rev. E **99**, 012421 (2019).
[21] M. Gilson, R. Moreno-Bote, A. Ponce-Alvarez, P. Ritter, and G. Deco, PLoS Comput. Biol. **12**, e1004762 (2016).
[22] E. S. C. Ching and H. C. Tam, Phys. Rev. E **95**, 010301(R) (2017).
[23] R. J. Prill, R. Vogel, G. A. Cecchi, G. Altan-Bonnet, and G. Stolovitzky, PLoS One **10**, e0125777 (2015).
[24] J. Ren, W.-X. Wang, B. Li, and Y.-C. Lai, Phys. Rev. Lett. **104**, 058701 (2010).
[25] S. L. Brunton, J. L. Proctor, and J. N. Kutz, Proc. Natl. Acad. Sci. USA **113**, 3932 (2016).
[26] W.-X. Wang, R. Yang, Y.-C. Lai, V. Kovanis, and M. A. F. Harrison, Europhys. Lett. **94**, 48006 (2011).
[27] W.-X. Wang, Y. C. Lai, and C. Grebogi, Phys. Rep. **644**, 1 (2016).
[28] G. Janashia, E. Lagvilava, and L. Ephremidze, IEEE Trans. Inf. Theory **57**, 2318 (2011).
[29] G. Janashia and E. Lagvilava, Studia Math. **137**, 93 (1999).
[30] L. Ephremidze, G. Janashia, and E. Lagvilava, Georgian Math. J. **15**, 241 (2008).
[31] P. Jezzard, P. M. Matthews, and S. M. Smith (eds.), *Functional MRI: An Introduction to Methods* (Oxford University, Oxford, 2001).
[32] D. Attwell and S. B. Laughlin, J. Cereb. Blood Flow Metab. **21**, 1133 (2001).
[33] K. M. Aquino, M. M. Schira, P. A. Robinson, P. M. Drysdale, and M. Breakspear, PLoS Comput. Biol. **8**, e1002435 (2012).
[34] P. A. Robinson, C. J. Rennie, and D. L. Rowe, Phys. Rev. E **65**, 041924 (2002).
[35] S. J. van Albada, C. C. Kerr, A. K. Chiang, C. J. Rennie, and P. A. Robinson, Clin. Neurophysiol. **121**, 21 (2010).
[36] N. Wiener and P. Masani, Acta Math. **98**, 111 (1957).
[37] P. A. Robinson, C. J. Rennie, and J. J. Wright, Phys. Rev. E **56**, 826 (1997).
[38] J. A. Roberts, A. Perry, A. R. Lord, G. Roberts, P. B. Mitchell, R. E. Smith, F. Calamante, and M. Breakspear, NeuroImage **145**, 379 (2016).
[39] G. Mehta-Pandejee, P. A. Robinson, J. A. Henderson, K. M. Aquino, and S. Sarkar, J. Neurosci. Methods **283**, 42 (2017).
[40] V. K. Jirsa and H. Haken, Phys. Rev. Lett. **77**, 960 (1996).
[41] J. Ockendon, S. Howison, A. Lacey, and A. Movchan, *Applied Partial Differential Equations*, revised ed. (Oxford University, Oxford, 2003), p. 113.
[42] K. J. Friston, L. Harrison, and W. Penny, NeuroImage **19**, 1273 (2003).
[43] M. L. Seghier and K. J. Friston, NeuroImage **68**, 181 (2013).